International Journal of Mass Spectrometry 277 (2008) 70–78

Contents lists available at ScienceDirect

International Journal of Mass Spectrometry

journal homepage: www.elsevier.com/locate/ijms

Electronic excitation of gaseous acetic acid studied by K-shell electron energy loss spectroscopy and *ab initio* calculations

Denis Duflot[a,*], Jean-Pierre Flament[a], Alexandre Giuliani[b,1], Jacques Heinesch[b], Marie-Jeanne Hubin-Franskin[b,2]

[a] *Laboratoire de Physique des Lasers, Atomes et Molécules (PhLAM), UMR CNRS 8523, Centre d'Études et de Recherches Lasers et Applications (CERLA, FR CNRS 2416), Université des Sciences et Technologies de Lille, F-59655 Villeneuve d'Ascq Cedex, France*

[b] *Université de Liège, Laboratoire de Spectroscopie d'Électrons diffusés, Institut de Chimie B6c, Sart Tilman, B4000 Liège 1, Belgium*

ARTICLE INFO

Article history:
Received 27 March 2008
Received in revised form 7 May 2008
Accepted 7 May 2008
Available online 15 May 2008

Keywords:
Acetic acid
K-shell excitation
Ab initio
Electron excitation

ABSTRACT

Ab initio Configuration Interaction calculations have been carried out in order to assign the bands observed in the carbon and oxygen K-shell spectra of gaseous acetic acid, measured using the inner-shell electron energy loss spectroscopy (ISEELS) method with better energy resolution than in previous studies. The good agreement between the theoretical and the measured spectra allows us to assign precisely most of the peaks, especially for the Rydberg states. Some of them have been shown to have strong valence character. The lowest energy band at the carbon edge is assigned to the transitions $1sC_1 \rightarrow 3p\pi/\sigma^*(C_1–H)$ and $1sC_1 \rightarrow \pi^*(C_2–O_2)$. Simple Franck–Condon calculations, based on the linear coupling approximation, were performed in order to reproduce the vibrational structure observed for the first time in the oxygen and carbon core excited species as well as in the previously measured X-ray photoelectron spectroscopy spectra of the core ionised molecule. Finally, the calculated structural parameters of the core states of acetic acid match well those of the corresponding valence states of their Z+1 molecules, as predicted by the equivalent core approximation. However, significant differences between the geometry of the $1sC_1 \rightarrow \pi^*(C_2–O_2)$ state and the CH_3NOOH ground state are obtained.

© 2008 Elsevier B.V. All rights reserved.

1. Introduction

Acetic acid (CH_3COOH), commonly known as vinegar, is produced in the human body as a result of alcohol oxidation after consumption of alcoholic beverages. It plays an important role in the metabolism processes of most forms of life and results naturally from the action of certain bacteria in foods or liquids containing sugars or ethanol.

Despite the fact that, after formic acid (HCOOH), acetic acid is the simplest organic acid, and is a major component of biological molecules, there are only a very few studies of its electronic states spectroscopy by inner shell excitation . The core ionisation energies have been measured by Naves de Brito et al. [1,2] using XPS methods. To our knowledge core excitation spectra have been reported by only one experimental study previously, namely inner-shell electron energy loss spectroscopy (ISEELS) in gas phase [3]. The energy resolution was about 0.6 eV. More recently, Urquhart and Ade [4] have performed a systematic comparison between measured and *ab initio* C1s,O1s $\rightarrow \pi^*(C_2–O_2)$ transitions energy in a large family of carbonyl compounds, including acetic acid but other transitions were not considered.

In the present work the electronic structure of acetic acid, and much more specifically the unoccupied levels, has been investigated by core shell excitation and *ab initio* calculations. Inner-shell electron energy loss spectroscopy has been used to record the C1s and O1s excitation spectra of acetic acid. The experimental conditions – high electron impact energy and quite small scattering angle – are such that electron energy loss spectra are expected to exhibit the same features with quite similar relative intensities as those of the corresponding ones in photoabsorption.

The goal of the present paper is to present a new ISEELS spectrum of acetic acid recorded with an apparatus resolution of 0.17 eV. In order to help in the assignment of the observed spectral features, *ab initio* calculations using Configuration Interaction (CI) techniques and vibrational analysis have been carried out. This paper is divided into the following sections: Section 2 describes

* Corresponding author. Tel.: +33 3 20 43 49 80; fax: +33 3 20 43 40 84.
E-mail address: denis.duflot@univ-lille1.fr (D. Duflot).
[1] Present address: DISCO Beamline, Synchrotron SOLEIL, BP 48, L'Orme des Merisiers, F-91192 Gif sur Yvette, France, and Cepia, Institut National de la Recherche Agronomique, BP 71627, F-44316 Nantes Cedex 3, France.
[2] Directeur de recherche du FRS-F.N.R.S.

1387-3806/$ – see front matter © 2008 Elsevier B.V. All rights reserved.
doi:10.1016/j.ijms.2008.05.006

the experimental set up; Section 3 deals with the computational method employed; the results are presented and discussed in Section 4 and finally, in Section 5 some conclusions are given.

2. Experimental

The inner-shell electron energy loss spectra were obtained with a Vacuum Science Workshop Ltd. (VSW) spectrometer which has been adapted for gas studies and high energy electron beams and has been equipped with a home-made position sensitive multi-detector system in order to improve data collection times. The experimental apparatus and procedure have been described in detail previously [5–7].

Briefly the spectrometer consists of an electrostatic 180° monochromator operating in the constant pass energy mode, a collision chamber and an electrostatic analyser identical to the monochromator. The monochromatised incident electrons are accelerated up to 2 keV and focused into the collision chamber using a four-element electron lens. The electrons are slightly deflected (0.02 radians) by two sets of *X*–*Y* plates inside the collision chamber. The scattered electrons are energy analysed and focused onto the entrance slit of the analyser by a lens similar to that used for acceleration.

In the collision conditions of low momentum transfer (i.e., high incident energy and small scattering angle), electric-dipolar transitions are primarily excited. Inside the vacuum vessel, a residual pressure of less than 1×10^{-8} mbar is maintained by a cryogenic pumping system. The electron gun and the analyser regions are differentially pumped by turbomolecular pumps respectively. The spectra have been recorded with 0.040 and 0.020 eV steps.

In order to take into account valence and lower energy inner shell excitation cross-section, a linear background has been subtracted from the raw spectra by extrapolating least square fit of the pre-edge experimental data.

The absolute energy scale has been calibrated at both edges relative to CO and the C1s → π* ($\nu' = 0$) band at 287.40 ± 0.02 eV and the O1s → π* transition at 534.21 ± 0.09 eV recording spectra with 0.01 eV steps [8].

The sample of acetic acid was purchased from VEL (Leuven, Belgium) and is quoted as having a minimum purity of 99.8%. It was used directly without further purification except for repetitive freeze–pump–thaw cycles in order to eliminate air and other volatile impurities in the sample.

3. Computational method

The computational method used in the present work is similar to that used in our previous study of the core excitation spectra of acrolein [9] with a few minor differences. The basic assumption is that core ion MO's (obtained at the ROHF-GVB level [10] with the GAMESS-US program [11]), are a better starting point than the ground state MO's for the calculation of the core excitation energies. Formally, these $E(1s \rightarrow i^*)$ core excitation energies may be written with respect to the $E(1s \rightarrow \infty)$ core ion energy in the following manner [12,13]:

$$E(1s \rightarrow i^*) = E(1s \rightarrow \infty) + \varepsilon_{i^*} + P_{i^*} + C_{i^*}$$

where ε_{i^*} is the mono-electronic energy of the i* virtual MO (Koopmans' theorem). The P_{i^*} and C_{i^*} terms represent the residual relaxation and correlation effects of the i* electron with respect to the core ion. In practice, relaxation is taken into account by diagonalisation of a CI matrix. The correlation term C_{i^*} is calculated by a multi-reference MP2 calculation with the three-class diagrammatic CIPSI [14,15] method and using the CI matrix eigenfunctions as zeroth-order wave-functions. In the present work, two types of CI calculations were performed:

(I) a preliminary calculation included all 1s → i* excitations from the core orbital to all virtual MO's. This type of calculations is sometimes called 1h–1p CI [16]. Physically, this means that the electron density of the core state is identical to that of the ion and relaxation is treated perturbatively during the CIPSI step together with correlation.
(II) a larger CI matrix including all mono-excitations with respect to all the 1s → i* core excitations was diagonalized (2h–2p scheme), taking explicitly into account relaxation effects and permitting the description of possible di-excited (shake up) states. In this case, in order to reduce the computational cost of the CIPSI step, the extrapolation procedure proposed by Angeli et al. [17] was employed, with 6 thresholds between 99.9 and 99.4%.

Finally, the theoretical dipolar electric intensities are obtained by evaluating the corresponding oscillator strengths (in the length gauge):

$$f_L = \frac{2}{3}\omega \left| \left\langle \Psi_{CI} \right| \mathbf{r} \left| \Psi_0 \right\rangle \right|^2$$

where ω is the transition energy, $\mathbf{r}$ the electric dipole transition moment, both in atomic units. ψ_{CI} and ψ_0 are the CI excited and ground state wave functions, respectively. The Gaussian atomic orbitals (AO's) used are the TZ2P basis set taken from Dunning [18]. The same exponents of the d polarization functions ($\alpha_C = 1.44$, 0.36 and $\alpha_O = 2.56$, 0.64) were used for the Z + 1 (equivalent core) atoms. For core-excited states, a set of Rydberg orbitals (5s, 5p, 3d) was added on the core excited atom. The exponents of the first diffuse AO's are taken from Dunning and Hay [19] and the other ones are obtained in an "even-tempered" manner. In the following, the extended basis set will be designated as TZ2P + R.

Then, in order to simulate the vibrational structure of some of the spectral bands, Franck–Condon factors calculations were carried out, using our local implementation [20,21] of the method proposed by Cederbaum and Domcke [22,23]. In its simplest form (linear coupling approximation), this model describes the potential energy surface of the excited state by the same harmonic oscilla-

Table 1
Core ionisation energies (eV) of acetic acid at the O1s and C1s edges

	C1s			O1s		
	C_1	C_2	Shift	O_1	O_2	Shift
Exp.[a]	291.55	295.38	3.83	540.09	538.29	−1.8
Exp.[b]	291.55(3)	295.35(3)	3.80	540.10(3)	538.31(3)	−1.79
ΔSCF[b]	292.49	296.96	4.47	541.03	538.80	−2.23
ΔSCF (GSCF3)[c]		296.52			537.70	
SA-MCQDPT[d]	288.32	293.02	4.70	532.38	530.31	−2.07
SA-MRMP[d]	288.21	292.36	4.15	530.10	528.98	−1.12
MRMP[d]	291.65	295.90	4.25	540.21	538.69	−1.52
ΔKS[e]	291.51	294.97	3.46	540.24	538.19	−2.05
ΔSCF[f]	292.00	296.39	4.39	540.07	537.87	−2.20
ΔMP2 (RMP)[f]	291.59	295.53	3.94	540.44	538.71	−1.73
ΔMP2 (ZAPT)[f]	291.60	295.55	3.95	540.44	538.71	−1.73
ΔMP2 (CIPSI)[f]	291.45	295.40	3.95	540.35	538.59	−1.76
ΔMP2 (CIPSI) + ZPVE[f]	291.09	295.24	4.15		538.36	

[a] Ref. [32].
[b] Refs. [1,2] (DZP basis set).
[c] Ref. [4].
[d] Ref. [30].
[e] Ref. [31] (Δ(PW86-PW91)/QZ4P//HF/6-31G* result with relativistic correction).
[f] This work. Values calculated at the TZ2P/MP2 optimized geometry using the TZ2P + Rydberg basis set.

tor as the ground state, the only difference being the equilibrium geometry. This model has proven to be satisfactory in the context of inner ionisation and excitation [24–26]. Thus, it is necessary to determine the gradient of the excitation energy E_{ex} at the ground state geometry:

$$\kappa_i = 2^{-1/2}\left(\frac{\partial E_{ex}}{\partial Q_i}\right)_0$$

This κ matrix has non-zero elements only for totally symmetrical modes (a' in the present case). These calculations were performed at the ROHF-GVB level for core states, because the more sophisticated methods widely used when dealing with valence states cannot be employed with core states (see for example Ref. [27]). Similarly, RHF geometry and frequencies were used for the ground state. Anharmonic frequencies were also calculated with the VSCF method [28] on a 40,000 points grid including 3-D couplings, as shown in the supplementary information. However, the anharmonic values could not be used because the Domcke–Cederbaum model is based on harmonic approximation. Therefore, the RHF harmonic frequencies were scaled by a factor of 0.9. The present calculations include hot bands, as well as combination bands, using a temperature of 298 K.

4. Results and discussion

In the following, the four heavy atoms of acetic acid will be labelled as $H_3C_1–C_2{=}O_2–O_1H$. The most stable isomer corresponds to an eclipsed conformation between $C_2{=}O_2$ and one of the $C_1{-}H$ bonds. As shown in the supplementary data, the calculated MP2 geometry are in better agreement with experiment [29] than the HF calculation and therefore, was used to calculate vertical core excitation energies. The electronic configuration is:

$$[1a'^2 2a'^2 3a'^2 4a'^2]5a'^2 6a'^2 7a'^2 8a'^2 9a'^2 10a'^2 1a''^2 11a'^2$$
$$12a'^2 2a''^2 3a''^2 13a'^2$$

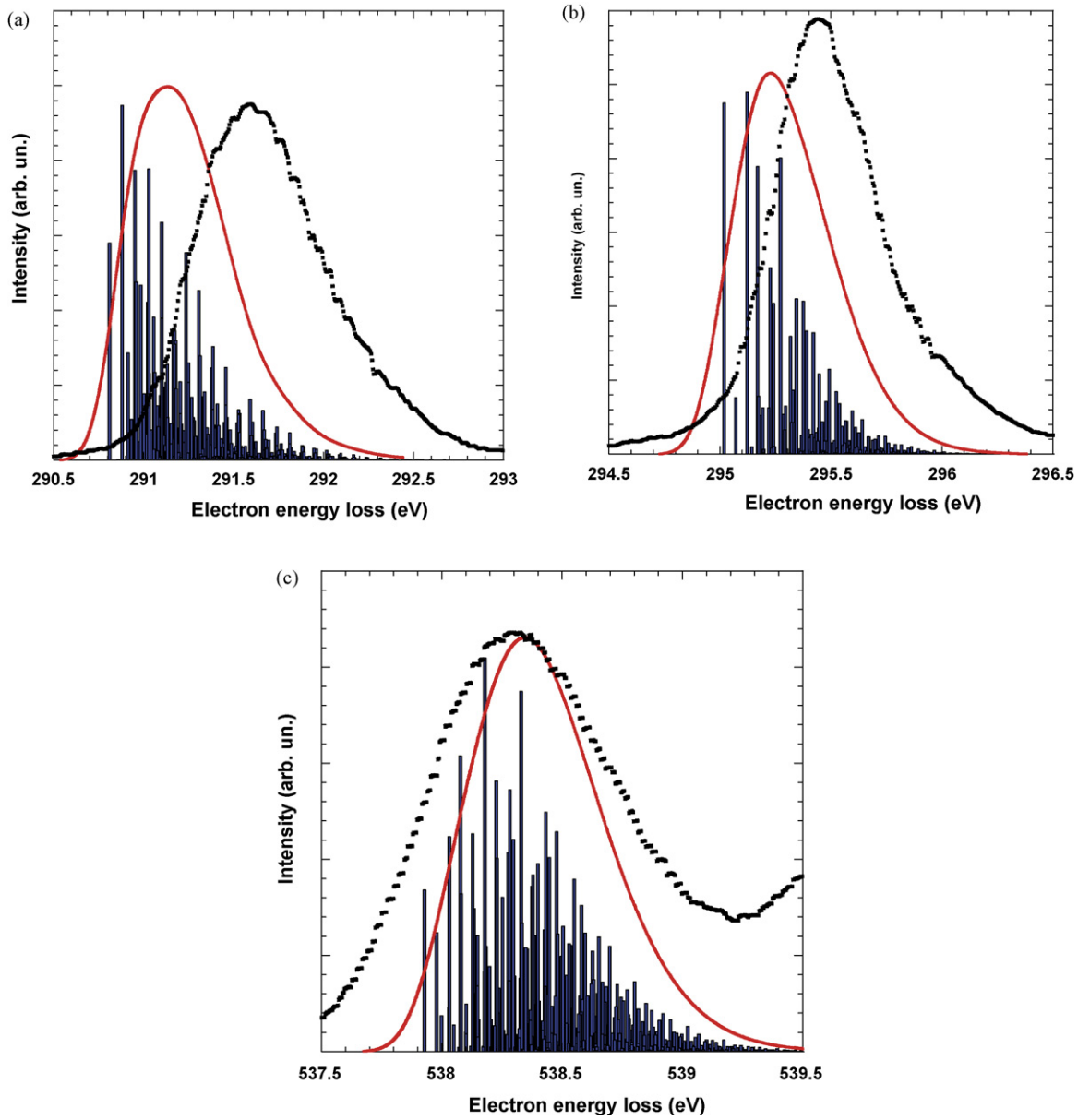

Fig. 1. Comparison of the calculated vibrational structure of the core ions with XPS: (a) C_1, (b) C_2, (c) O_2. Dots: experiment from Ref. [2]; sticks: calculated vibrational transitions; line: total calculated vibration spectrum, using FWHM = 0.25 eV gaussian functions.

where the bracketed MO's correspond to the O_1, O_2, C_2 and C_1 core 1s orbitals, respectively. The HOMO 13a′ is essentially the in-plane O_2 lone pair (the "plane" being defined as $C_1C_2O_1O_2$). The SHOMO 3a″ is the $\pi(C_2–O_2)$ and has an anti-bonding character with the out-of-plane O_1 lone pair. The LUMO corresponds to the $\sigma^*(O_1–H)$ MO, the $\pi^*(C_2–O_2)$ being higher in energy.

4.1. Core ionisation energies

The calculated core ionisation energies are compared with theoretical [2,4,30,31] and experimental [1,32] determinations in Table 1. Since several possible definitions of the zero-order hamiltonian are possible in open-shell MP2 calculations [33], the ΔMP2 values were obtained using three different models: RMP [34,35], ZAPT [36,37], and CIPSI.

Our ΔSCF values are close to the ΔSCF/GSCF3 ones [4]: the C_1 and C_2 energies are too large, while the O_1 values are close to experiment and the O_2 values are too low by ∼1 eV. On the other hand, the ΔSCF values of Naves de Brito et al. [2] are rather different, with a 1.6 eV error for C_2. These authors have discussed in detail the possibility that the zero-point vibrational energy (ZPVE) correction could be responsible of this effect. However, both the present and GSCF3 [4] results suggest basis set effects. At the correlated level, the ΔKS values of Takahata and Chong [31] are in very good agreement with experiment, except for C_2 where the result is too low by ∼0.5 eV. Shirai et al. [30] have shown the complete failure of State-Averaged (SA) multiconfigurational calculations, especially for the oxygen atoms where the calculated values differ by ∼10 eV from experiment.

For the three ΔMP2 methods of the present work, the agreement with experiment is within a few tenths of an eV, especially for carbons. Our mono-reference MP2 results also compare well with the MRMP results of Shirai et al. [30]. All the ΔSCF chemical shifts are also too large, while the MP2 ones are in excellent agreement with experiment. In the following, the CIPSI values will be used in order to be consistent with the core excitation energy calculations.

Concerning possible vibrational effects, Naves de Brito et al. [2] simply subtracted the ground state zero-point energy from their ΔSCF ionisation energies to explain the discrepancies with experiments. They pointed out that a complete normal mode analysis would be necessary to determine the "appropriate fraction" of the ZPVE to be removed. Using the simple vibrational model described in the previous section, such an analysis was done. The results of Fig. 1 show the comparison with the experimental spectra [1,2]. The vibrational structure being not discernible in the XPS spectrum [1,2], a FWHM of 0.25 eV was used for the vibrational bands. It should be noticed that since the O_1 core ion state was found to be dissociative (see Section 4.4), such an analysis is meaningless. This is consistent with the fact that the O1 XPS band has the largest FWHM (1.20 eV) [2] of the four atoms. The shape of the bands is correctly reproduced and the calculated half-widths (0.66 eV for C_1, 0.50 eV for C_2 and 0.66 eV for O_2) are close to the experiment [2] (0.83 eV for C_1 and 0.58 eV for C_2), except for O_2 where the 1.04 eV measured value may be too large because of the overlapping of the O_1 band at high energy. According to the authors [2], these observed widths of the XPS bands are mainly due to spectrometer resolution and vibrational broadening, both effects approximated by a single asymmetric gaussian profile, while lifetime broadening is much smaller. The vibrational analysis also shows that the 0–0 band origin is always below the calculated vertical energy (0.58 eV for C_1, 0.34 eV for C_2 and 0.60 eV for O_2). Moreover, the maximum of the total band does not correspond to the 0–0 transition, because of the numerous vibrational peaks. Assuming the maximum of each band in Fig. 1 should give the "ZPVE-corrected" ionisation energy, the resulting values, given in the last line of Table 1, are very close to experiment for C_2 and O_2, while the C_1 ionisation energy is too large by 0.5 eV. The origin of this discrepancy may come from the fact that we used the calculated CIPSI values for the vertical ionisation energies. As recently reviewed by Carniato and Luo [13], various terms other than ZPVE, may play a role in the calculation of core ionisation energies, leading to an accuracy of a few tenths of an eV. For example, the relativistic correction could slightly alter the calculations. However, according to Takahata and Chong [31], this correction is only 0.05 eV for carbons and 0.20 eV for oxygens.

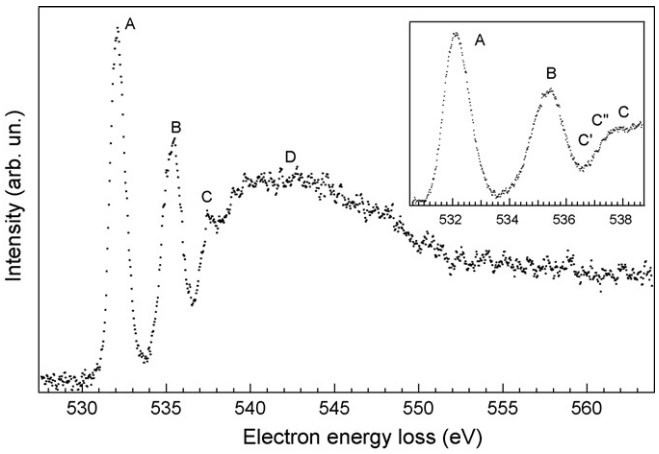

Fig. 2. The electron energy-loss spectrum of acetic acid recorded at the oxygen K edge with an energy resolution of 0.17 eV and 40 meV steps. Insert: The excitation spectrum in the 530.6–538.7 eV region is recorded with 20 meV steps.

4.2. Oxygen K-shell electron-energy loss spectrum

The O1s edge electron energy loss spectrum of acetic acid is shown in Fig. 2, while the energies of the observed bands are indicated in Table 2. To the best of our knowledge, the only other available ISEELS spectrum was published by Robin et al. [3] with a resolution of 0.6 eV. The two spectra are in agreement but the

Table 2
Energies (eV) of the spectral features in the ISEELS spectra

O1s	This work	ISEELS[a]	Assignment[a]	
			O_1	O_2
A	532.10	531.95		$1\pi^*(\pi^*(C_2–O_2))$
B	535.35	535.2	$1\pi^*(\pi^*(C_2–O_2))$	3p
C′	537.04			
C″	537.36			
C	537.90	537.6	$3p/\sigma^*(O_1–H)$	Rydberg
D	541.40	541.4(8)	$\sigma^*(C_1–C_2)$	$\sigma^*(C_2–O_1)$
		543.5(8)	$\sigma^*(C_2–O_1)$	
		546.3(8)	$\sigma C_2{=}O_2)$	

C1s	This work	ISEELS[a]	Assignment[a]	
			C_1	C_2
A	287.8	287.4	3s	
B[b]	288.74	288.69	$3p/\sigma^*(C_1–H)$	$1\pi^*(\pi^*(C_2–O_2))$
C	290.56	290.3	4p	
C′	291.64	291.5		3s
D[c]	293.60	293.4	$\sigma^*(C_1–C_2)$	3p
D′	294.35	294.6		4p
E	297.35	297.3		$\sigma^*(C_1–C_2)$
F	302.7	303.1(5)		$\sigma^*(C_2–O_2)$

[a] Ref. [3].
[b] Band B: on the high energy side a low intensity feature not well resolved at 289.4 eV.
[c] Band D: fine features not well resolved at 293.38 and 293.84 eV.

Table 3
Calculated energies and relative intensities of the O1s core excited states of acetic acid

State	E (eV)	TV (eV)		Intensity[a]	Main configurations		$\langle r^2 \rangle$ (a.u.^{2})
		O_1	O_2		O_1	O_2	
A″	532.29		6.29	1.000[b]		0.92 $1sO_2 \rightarrow \pi^*(C_2–O_2)$	52
A′	534.82		3.77	0.020		0.97 $1sO_2 \rightarrow 3s\sigma$	107
A″	535.52	4.83		0.334	0.92 $1sO_1 \rightarrow \pi^*(C_2–O_2)$		50
A′	535.78	4.56		0.303	0.97 $1sO_1 \rightarrow 3s\sigma/\sigma^*(O_1–H)$		93
A′	535.81		2.78	0.048		0.98 $1sO_2 \rightarrow 3p\sigma$	123
A″	536.09		2.49	0.034		0.98 $1sO_2 \rightarrow 3p\pi$	138
A′	537.20		1.39	0.021		0.98 $1sO_2 \rightarrow 4s\sigma$	440
A″	537.24		1.35	0.027		0.98 $1sO_2 \rightarrow 4p\pi$	387
A′	537.39	2.96		0.113	0.98 $1sO_1 \rightarrow 3p\sigma/\sigma^*(O_1–H)$		101
A″	537.70	2.64		0.072	0.98 $1sO_1 \rightarrow 3p\pi$		123
A′	537.92	2.42		0.033	0.98 $1sO_1 \rightarrow 3p\sigma'$		147
A′	538.35	2.00		0.061	0.97 $1sO_1 \rightarrow 3d\sigma$		225
	538.59[c]		0.00			Ion O_2	
A′	538.91	1.43		0.039	0.98 $1sO_1 \rightarrow 4p\sigma$		423
A″	538.92	1.42		0.036	0.99 $1sO_1 \rightarrow 4p\pi$		356
A′	539.03	1.31		0.022	0.99 $1sO_1 \rightarrow 4p\sigma'$		506
	540.35[c]	0.00			Ion O_1		

[a] Relative oscillator strength to the most intense peak.
[b] Absolute calculated oscillator strength $f = 0.0280$.
[c] ΔMP2(CIPSI)/TZ2P + R//MP2/TZ2P level.

higher resolution of the present work shows some fine features (C, C′ and C″) below the O_2 threshold. The assignments proposed by Robin et al. [3] are also given in Table 2. The spectrum is dominated by two broad bands A and B, centred at 532.10 and 535.35 eV, respectively.

The results of the calculations are shown in Table 3. Only the 2h–2p values with a relative intensity of 2% of the most intense peak are given (the complete table may be found in the supporting information). The spectra derived from the two types of calculations (1h–1p and 2h–2p) are given in Fig. 3a and b (the calculated bands were convoluted using 0.17 eV FWHM gaussian functions). Both CIPSI methods give very similar results. This is not surprising since all calculated core states wave functions are dominated by a single mono-excitation. As proposed earlier [3], the first band A is assigned to the $1sO_2 \rightarrow \pi^*(C_2–O_2)$. The characteristics (energy, Term Value and oscillator strength) of this transition, are compared to experiment in Table 4. The GSCF3 results [4] overestimate the core excitation energy, due to the frozen core approximation used [38]. On the other hand, the present ROHF-GVB energy is underestimated, but the TV is correct. The two CIPSI values, using the 1h–1p and 2h–2p models, give nearly identical results, in much better agreement with experiment. In particular, the calculated absolute oscillator strengths (0.0303 and 0.0280) are in very good agreement with the measured values [3] of 2.9×10^{-2} while the GSCF3 value of 0.0149 are too low.

Table 4
Transition energies, Term Values and oscillator strengths of the two most intense bands at different levels of theory

	$1sO_2 \rightarrow \pi^*(C_2–O_2)$			$1sC_2 \rightarrow \pi^*(C_2–O_2)$		
	E (eV)	TV (eV)	f	E (eV)	TV (eV)	f
GSCF3[a]	533.29	4.40	0.0149	291.37	5.15	0.0715
ROHF-GVB[b]	531.62	6.25		289.41	6.98	
CIPSI (1h–1p)[b]	532.23	6.35	0.0303	288.43	6.96	0.0829
CIPSI (2h–2p)[b]	532.29	6.29	0.0280	288.60	6.80	0.0920
Exp.[c]	532.10	6.21	0.029	288.74	6.61	0.104

[a] Ref. [4].
[b] This work.
[c] This work with Refs. [3,1].

The rather large width of the A band (FWHM ≈ 1.0 eV) suggests the presence of vibrational excitation, although it is not resolved. Another possible cause of broadening for band A could be a small contribution due to O1s transitions from dimerised acetic acid. However, such a contribution would be very unlikely at the pressures used in the present experiment. The results of the vibration calculations are compared to experiment in Fig. 4a. The agreement is rather good and the general shape of this band is well reproduced. Not surprisingly, the structure is mainly due to the $C_2–O_2$ stretching mode (1987 cm^{-1}). Other totally symmetric bending modes are also excited. These results were confirmed by calculating the equilibrium geometry of the $1sO_2 \rightarrow \pi^*(C_2–O_2)$ core excited state at the ROHF-GVB level, as shown in Table 5 and supplementary data. When compared to the RHF ground state geometry, the $C_2–O_2$ bond is weakened and the length increases from 1.1816 to 1.3435 Å, close to the $C_2–O_1$ single bond value. Moreover, the $\pi^*(C_2–O_2)$ HOMO is mainly concentrated on the C_2 atom and has a sp^3 contribution from C_1. This causes the pyramidalisation of the COOH group, with the angles between the four heavy atoms close to 109°, much as in the methyl group. Another peculiarity is the fact that the C_1, C_2, O_1 and H atoms nearly lie in the same plane. Remarkably, the geometry of the ground state of CH_3CFOH, which is the "Z + 1" equivalent of acetic acid, is almost perfectly identical, confirming the equivalent core approximation.

The second band B of the spectrum has its maximum at 535.35 eV and is wider than band A (FWHM ≈ 1.5 eV), suggesting the presence of more than one transition. It was assigned [3] to the $1sO_1 \rightarrow \pi^*(C_2–O_2)$ and $1sO_2 \rightarrow 3p$ Rydberg transitions (Table 2). This is confirmed by the present calculations, since the $1sO_1 \rightarrow \pi^*(C_2–O_2)$ transition is calculated to occur at 535.52 eV with a relative intensity of 33% of the first peak A (Table 3). This rather high intensity may be rationalised by the fact that the $\pi^*(C_2–O_2)$ MO is slightly delocalised on the O_1 atom. The three $1sO_2 \rightarrow 3p$ Rydberg transitions are predicted to occur at 535.81, 536.09 and 536.28 eV, i.e., on the high energy tail of the band, while the $1sO_2 \rightarrow 3s\sigma$ is calculated on the low energy side, at 534.82 eV. However, the calculated intensities for these four transitions are small (<5%) so that their contributions to the B band should be weak. On the other hand, the calculations predict the $1sO_1 \rightarrow 3s\sigma$ transition to occur at 535.78 eV with an intensity of 30% (Table 3). The

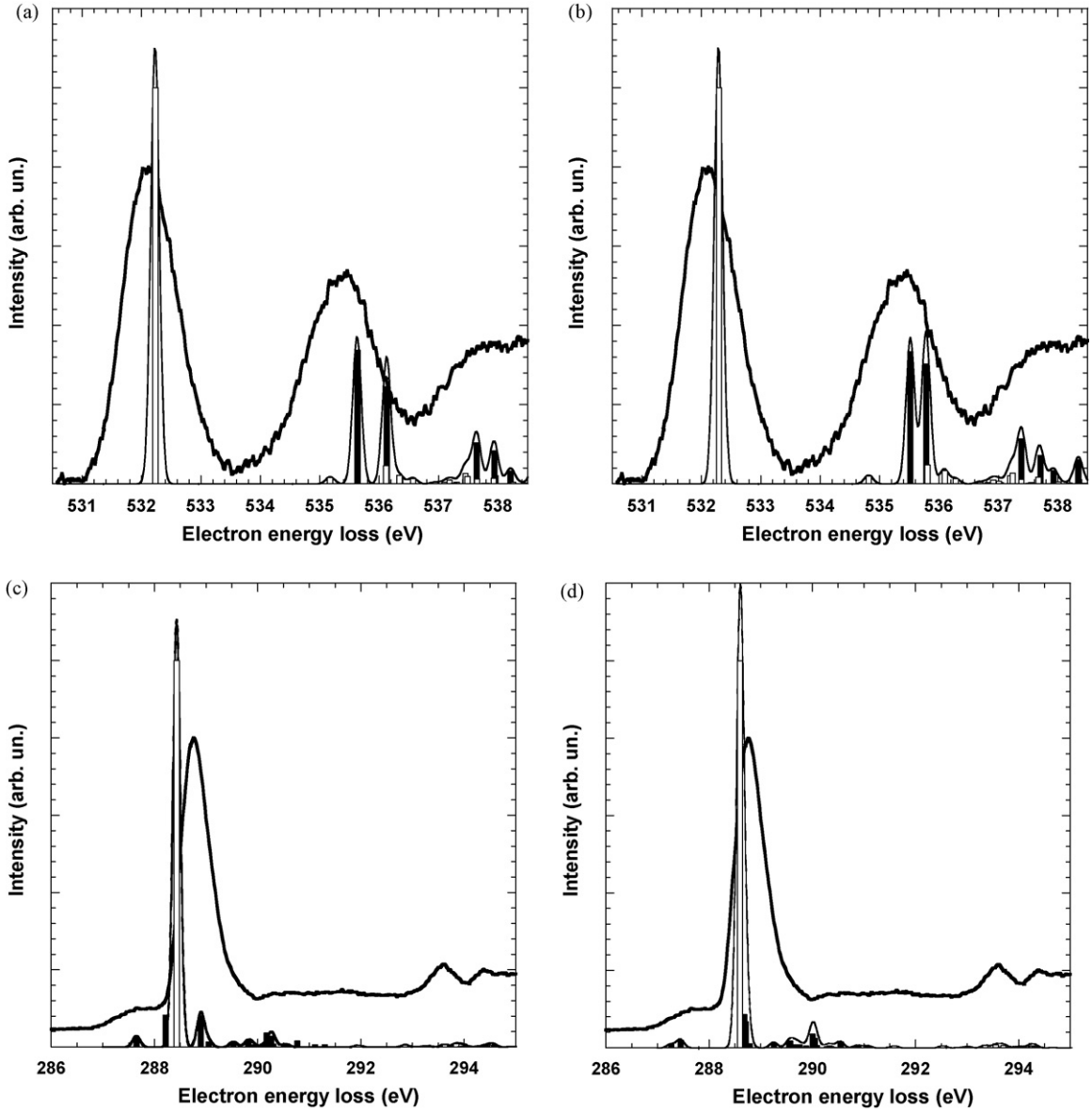

Fig. 3. Comparison between the experimental and the theoretical spectra (FWHM = 0.17 eV) for the pre-edge regions (white: O_1 and C_2, black: O_2 and C_1): (a) O1s 1h–1p calculations, (b) O1s 2h–2p calculations, (c) C1s 1h–1p calculations, (d) C1s 2h–2p calculations.

contrast in the intensities of the 3sσ transitions for the two O atoms may be explained by the important $\sigma^*(O_1–H)$ valence character of the 3sσ MO for O_1. To summarise, the B band is mainly due to the $1sO_1 \rightarrow \pi^*(C_2–O_2)$ and $1sO_1 \rightarrow 3s\sigma/\sigma^*(O_1–H)$ transitions, having very similar energies and intensities, and with minor contributions of O_2 3s and 3p Rydberg transitions.

As for band A, it is possible that vibrational excitation contributes to the width of band B. However, the geometry optimisation of the two $1sO_1$ states (at ROHF-GVB level) showed that both states are unstable (Table 5): the $3s\sigma/\sigma^*(O_1–H)$ state dissociates into $CH_3COO + H$, while the $\pi^*(C_2–O_2)$ state dissociates into $CH_3CO + OH$. For the first state, the $\sigma^*(O_1–H)$ valence character of the 3sσ MO is consistent with the O_1–H bond breaking. For the second state, the breaking of the C_2O_1 bond, rather than the C_2O_2 one, may be due to the delocalised nature of the π^* MO on the O_1 atom. The same state of the CH_3COFH Z + 1 equivalent molecule exhibits the same behaviour with an important qualitative difference in the Mulliken charges: the π^* states dissociates into $HF^- + CH_3CO^+$ fragments (Table 5). The dissociative nature of these two states proves that the B band of the K-shell spectrum should exhibit a continuum, even at a better resolution.

At higher energy, the observed spectrum does not show any discernible band, since the intensity increases monotonously until the O_2 ionisation threshold is reached around 538.5 eV (Fig. 2). This is consistent with the calculations, predicting the O_2 Rydberg transitions to occur above 536 eV (Table 3). All these transitions are purely Rydberg with very small intensities. They are probably responsible for the weak feature C′ located at 537.04 eV. On the other hand, the C″ feature measured at 537.36 eV corresponds to the $1sO_1 \rightarrow 3p\sigma/\sigma^*(O_1–H)$, calculated at 537.39 eV. As for the 3sσ transition, its high intensity (11%) is due to its important valence character. The C feature at 537.90 eV is assigned to the $1sO_1 \rightarrow 3p\pi$ transition, calculated at 537.70 eV, with a rather high intensity (7%) due to a small valence character.

The next energy region of the spectrum corresponds to the O1 ionisation continuum. Robin et al. [3] distinguished three features

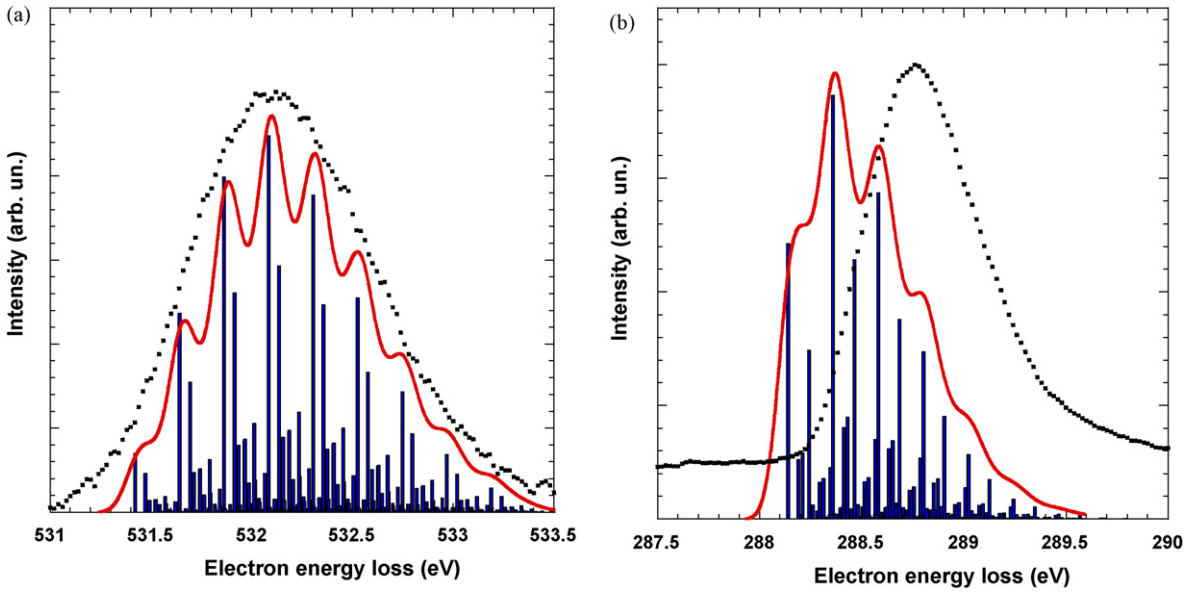

Fig. 4. Calculated vibrational structure (FWHM = 0.17 eV gaussian functions) compared to experiment. (a) Band A, O1s edge, (b) band B, C1s edge.

at 541.4, 543.5 and 546.3 eV (Table 2), assigned to O_1 shape resonances, but only the first one seems to be present in the spectrum of Fig. 3. The calculations reported in Table 3 predict O_1 Rydberg transitions to occur at such energies with weak intensities. However, the present theoretical model does not allow a proper description of transitions beyond the ionisation threshold.

4.3. Carbon K-shell electron-energy loss spectrum

The C1s electron energy loss spectrum is shown in Fig. 5 and the energies of the peaks are collected in Table 2, together with the results of the previous study of Robin et al. [3]. The spectrum is dominated by a strong band B, centred at 288.74 eV, which is highly asymmetric on the high energy side. The A band, which appeared only as weak shoulder in Robin's spectrum, is now clearly discernible at 287.8 eV. Above 290 eV, the spectrum is nearly flat with two weak features C (290.56 eV) and C' (291.64 eV).

The most intense (>1%) calculated transitions (2h–2p level) are displayed in Table 6, while the theoretical spectra obtained at both 1h–1p and 2h–2p levels are compared to the experiment in Fig. 3c and 3d. As in the O1s case, for nearly all calculated core excited states, the CI wave function is dominated by a single mono-excitation (weight >91%). There is however an important exception: the two lowest lying A "C_1 transitions, corresponding to transitions to the $3p\pi/\sigma^*(C_1–H)$ and $\pi^*(C_2–O_2)$ MO's. At the 1h–1p level, these transitions are calculated at the same energy (288.22 and 288.23 eV, respectively), although with different intensities: 8% for $1sC_1 \rightarrow 3p\pi/\sigma^*(C_1–H)$ and less than 0.1% for $1sC_1 \rightarrow \pi^*(C_2–O_2)$. These intensities are consistent with the fact that the $3p\pi$ MO has an important $\sigma^*(C_1–H)$ valence character, while the $\pi^*(C_2–O_2)$ MO

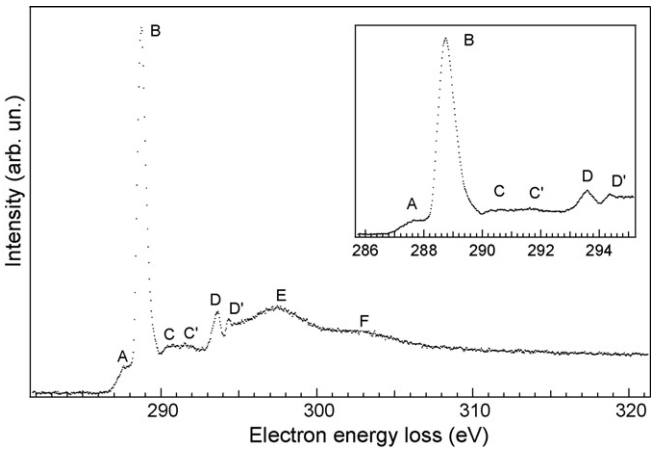

Fig. 5. The electron energy-loss spectrum of acetic acid recorded at the carbon K edge with an energy resolution of 0.17 eV and 40 meV steps. Insert: The excitation spectrum in the 285.8–295.2 eV region recorded with 20 meV steps.

Table 5
Stability of core ionised and excited states of acetic acid and corresponding states of Z + 1 molecules

Acetic acid		Core states	Z + 1 molecule	Valence states		
Ion O_1	$^2A'$	$C_1H_3C_2O_2 + O_1H^+$	CH_3COFH^+	Ion O_1	$^1A'$	$CH_3CO^+ + FH$
Ion O_2	$^2A'$	Stable	CH_3CFOH^+	Ion O_2	$^1A'$	Stable
Ion C_1	$^2A'$	Stable	NH_3COOH^+	Ion C_1	$^1A'$	Stable
Ion C_2	$^2A'$	Stable	CH_3NOOH^+	Ion C_2	$^1A'$	Stable
$1sO_1 \rightarrow \pi^*(C_2–O_2)$	$^1A''$	$C_1H_3C_2O_2 + O_1$ H	CH_3COFH	$\pi^*(C_2–O_2)$	$^2A''$	$CH_3CO^+ + FH^-$
$1sO_1 \rightarrow 3s\sigma/\sigma^*(O_1–H)$	$^1A'$	$C_1H_3C_2O_2O_1 + H$		$3s\sigma/\sigma^*(F–H)$	$^2A'$	$CH_3COF + H$
$1sO_2 \rightarrow \pi^*(C_2–O_2)$	^1A	Stable	CH_3CFOH	$\pi^*(C_2–F)$	^2A	Stable
$1sO_2 \rightarrow 3s\sigma$	$^1A'$	$C_1H_3C_2O_2O_1 + H$		$3s\sigma$	$^2A'$	$CH_3CFO + H$
$1sC_1 \rightarrow 3s\sigma/\sigma^*(C_1–H)$	$^1A'$	Stable	NH_3COOH	$3s\sigma/\sigma^*(N–H)$	$^2A'$	Stable
$1sC_1 \rightarrow \pi^*(C_2–O_2)$		$C_1H_3 + C_2O_2O_1H$		$\pi^*(C_2–O_2)$		$NH_3 + COOH$
$1sC_2 \rightarrow \pi^*(C_2–O_2)$	^1A	Stable	CH_3NOOH	$\pi^*(N–O_2)$	^2A	Stable
$1sC_2 \rightarrow 3s\sigma$	$^1A'$	Stable		$3s\sigma$	$^2A'$	Stable

Table 6
Calculated energies and relative intensities of the C1s core excited states of acetic acid

State	E (eV)	TV (eV)		Intensity[a]	Main configurations		$\langle r^2 \rangle$ (a.u.^{2})
		C_1	C_2		C_1	C_2	
A″	287.27	4.18		0.009	0.39 $1sC_1 \rightarrow 3p\pi/\sigma^*(C_1–H)$ +0.48 $1sC_1 \rightarrow \pi^*(C_2–O_2)$		64
A′	287.45	4.00		0.021	0.98 $1sC_1 \rightarrow 3s\sigma$		82
A″	288.60		6.80	1.000[b]		0.91 $1sC_2 \rightarrow \pi^*(C_2–O_2)$	55
A′	288.68	2.77		0.087	0.98 $1sC_1 \rightarrow 3p\sigma/\sigma^*(C_1–H)$		105
A″	288.71	2.74		0.068	0.58 $1sC_1 \rightarrow 3p\pi/\sigma^*(C_1–H)$ 0.39 $1sC_1 \rightarrow \pi^*(C_2–O_2)$		105
A″	290.01	1.44		0.035	0.96 $1sC_1 \rightarrow 4p\pi$		324
A′	290.05	1.40		0.024	0.98 $1sC_1 \rightarrow 4p\sigma'$		343
	291.45[c]	0.00			Ion C_1		
	295.40[c]		0.00			Ion C_2	

[a] Relative oscillator strength to the most intense peak.
[b] Absolute calculated oscillator strength $f = 0.0920$.
[c] ΔMP2(CIPSI)/TZ2P + R//MP2/TZ2P level.

is mainly localised on C_2 and O_2. At the 2h–2p level (Table 6), the results are somewhat different: the first A" transition is now predicted at 287.27 eV with an intensity of 0.9%, while the second one is calculated at 288.71 eV with an intensity of 6.8%. Thus, the splitting between the two states is now 1.44 eV. For both states, the CI wave functions show a strong mixing between the $1sC_1 \rightarrow 3p\pi/\sigma^*(C_1–H)$ and $1sC_1 \rightarrow \pi^*(C_2–O_2)$ excitations. As shown by Löwdin [39], it is possible to construct from these wave functions the so-called "natural orbitals", after diagonalisation of the CI density matrix. The resulting MO's represent the best approximations of the "true" core excited MO's (see supplementary data). Both transitions appear to be mono-electronic, with 1s and virtual MO's having occupation numbers close to 1. The first transition can be viewed as the $1sC_1 \rightarrow \pi^*(C_2–O_2)$, while the second one is the $1sC_1 \rightarrow 3p\pi/\sigma^*(C_1–H)$ transition. These assignments are consistent with the calculated $\langle r^2 \rangle$ values: 64 a.u.^{2} for the first one, typical of a valence transition and 105 a.u.^{2} for the second one, close to the two other 3p values. Moreover, the fact that the energy of the second transition is close to the two other 3p transitions supports these assignments.

Using these results, it appears that the weak band A observed in the spectrum at 287.8 eV is assigned not only to the $1sC1 \rightarrow 3s\sigma$ transition, as proposed by Robin et al. [3], but also to the $1sC1 \rightarrow \pi^*(C_2–O_2)$, both having low intensities (Table 6). The next band B is assigned mainly to the intense $1sC_2 \rightarrow \pi^*(C_2–O_2)$ transition, with contributions from the $1sC_1 \rightarrow 3p$ transitions calculated at the same energy. In particular, two 3p transitions have non negligible intensities, due to their Rydberg-valence character: the $1sC_1 \rightarrow 3p\sigma/\sigma^*(C_1–H)$ (8.7%) and the $1sC_1 \rightarrow 3p\pi/\sigma^*(C_1–H)$ (6.8%). Together with the 3d states predicted around 289.5 eV, they are responsible of the asymmetry observed on the high energy side of the B band. Another possible cause of the asymmetry may be vibrational excitation. Fig. 4b compares with experiment the vibrational fine structure of the $1sC_2 \rightarrow \pi^*(C_2–O_2)$ transition, calculated at the ROHF-GVB level. It should be kept in mind that the vibration contributions of the $1sC_1$ transitions present in this region are not included. The asymmetry is well reproduced, although the maximum of the calculated band is 0.3 eV below the experimental maximum. This discrepancy is partially due to the difference between the calculated (288.60 eV) and the measured (288.74 eV) vertical ionisation energies.

The parameters of the intense $1sC_2 \rightarrow \pi^*(C_2–O_2)$ transition, obtained using various methods, are shown in Table 4. The behaviour of the different theoretical methods is essentially the same as for the $1sO_2 \rightarrow \pi^*(C_2–O_2)$ transition, the best results being obtained with CIPSI. Because of the mono-electronic nature of this transition, the 1h–1p and 2h–2p are almost identical. The CIPSI calculated absolute oscillator strengths (0.0829 and 0.0920) are in very good agreement with the measured values of 10.4×10^{-2} measured by Robin et al. [3] while the GSCF3 value of 0.0715 is slightly too small.

According to the calculations, the next energy region, between 290 and 291.5 eV, corresponds to Rydberg transitions from the C_1 atom. Most of these transitions are purely Rydberg and have thus very low intensities, with the exception of two 4p transitions predicted at 290 eV whose MO's have a slight valence character and who are responsible for the feature C observed at 290.56 eV. The C′ at 291.64 eV may be due to the C_1 ionisation threshold at 291.45 eV. At higher energies, the calculations predict the C_2 Rydberg transitions to occur. According to Table 2 and Fig. 3d, there seems to be a good agreement between the position of the D (293.60 eV) and D′ (294.35 eV) bands and some of these transitions. However, these results must be considered with caution, because of the possible coupling between the C_1 continuum and the C_2 Rydberg transitions, which has not been taken into account by the calculations. Moreover, these features may also be due to (above threshold) C_1 transitions. Finally, the two last observed features E (297.35 eV) and F (302.7 eV) are assigned to possible shape resonances.

4.4. Geometry of core states of acetic acid

Due to the variational collapse of the core hole wave function, standard correlated methods cannot be employed to optimise the geometry of core excited states, especially for polyatomic molecules. Therefore, the geometry of core states of acetic acid were obtained at the ROHF-GVB level, as implemented in the GAMESS-US package, and compared to their Z + 1 counterparts. The main results are given in Table 5. The case of the $1s\ O_2 \rightarrow \pi^*(C_2–O_2)$ transition has already been discussed in detail above. Qualitatively, the Z + 1 approximation gives results identical to the core calculations. The only difference resides in the Mulliken charge repartition for the dissociation products of the O_1 ion and $1s\ O_1 \rightarrow \pi^*(C_2–O_2)$ state. Detailed structural information may be found in the supplementary material of this paper. For all the optimised states, the Z + 1 and core angles are identical within 0.1°, except for a few dihedral angles. The bond lengths are also identical within 0.01 Å. This agreement is fully consistent with the results obtained in the case of core excited

cyclopropane [26]. There is however one exception, concerning the 1s $C_2 \rightarrow \pi^*(C_2–O_2)$ state, where the Z + 1 model give results qualitatively different from the core states: while both molecules appear to be pyramidalised at the C_2 atom, the orientation of the O_1–H bond is completely different. One possible explanation would be that both geometries correspond to two different minima of the potential energy surfaces of the two molecules. However, this is not confirmed by the calculations. One has to conclude that in this particular example, the equivalent core model fails to predict the "true" core result. Similar discrepancies have been found in the case of core excited benzene [40] and aniline [41]. The differences seem to involve mainly the lowest frequency modes, such as the O_1–H torsion in acetic acid, or the rotation of the NH_2 group in aniline [41].

The results of Table 5 are also another example of the selectivity of bond breaking upon core excitation, such as in the recent case of $\sigma^*(COCH_3)$ MO of ester thin films [42–44]. The results have been rationalised by calculating the core state energy gradient in the Franck–Condon region of the ground state [45]. Finally, the fragment products of C1s excited acetic acid have been studied experimentally [46,47]. Several dissociation channels involving ion pairs were found and these results may seem contradictory with the calculations shown in Table 5 where core states appear to be stable or giving neutral fragment. There are two possible explanations for this discrepancy: the experimental method cannot detect neutral species. Moreover, the fragments observed are probably due to the valence CH_3COOH^{++} dication which is the results of the Auger decay of the core states.

5. Conclusions

In this work, the core excitation spectra of gaseous acetic acid have been measured and interpreted using *ab initio* Configuration Interaction and simple Franck–Condon calculations based on the linear coupling approximation at both edges. The spectra have been recorded by high energy electron impact in electric dipolar interaction conditions, with a higher resolution than in previous works. The calculations allow a precise assignment of most observed bands and show that most core states are well described by a monoelectronic representation. Vibrational excitation in the first band at the C1s and O1s edges, respectively, have been observed for the first time. This vibrational fine structure looks quite similar to that of the ions observed in the X-ray photoelectron spectrum and both are well reproduced by simple Franck–Condon calculations. Finally, the calculated core states geometries are found to be close to their equivalent core counterparts. Some exceptions occur when low vibrational modes are involved, leading to qualitatively different geometries.

Acknowledgements

The "Laboratoire de Physique des Lasers, Atomes et Molécules" (PhLAM) is "Unité Mixte de Recherche du CNRS". The "Centre d'Études et de Recherches Lasers et Applications" (CERLA, FR CNRS 2416), is supported by the "Ministère chargé de la Recherche", the "Région Nord/Pas-de-Calais" and the "Fonds Européen de Développement Économique des Régions" (FEDER). Part of the computations were carried out at the CRI (Centre de Ressources Informatiques), on the IBM computer which is supported by the "Programme de Calcul Intensif et Parallèle" of the "Ministère chargé de la Recherche", the "Région Nord/Pas-de-Calais" and the FEDER. This research has been supported by the Fonds de la Recherche Scientifique (FRS-FNRS) and the Patrimoine of the Université de Liège. M.-J. Hubin-Franskin wishes to acknowledge the Fonds de la Recherche Scientifique for her research position.

Appendix A. Supplementary data

Supplementary data associated with this article can be found, in the online version, at doi:10.1016/j.ijms.2008.05.006.

References

[1] A. Naves de Brito, M.P. Keane, N. Correia, S. Svensson, U. Gelius, B.J. Lindberg, Surf. Interface Anal. 17 (1991) 94.
[2] A. Naves de Brito, N. Correia, S. Svensson, H. Agren, J. Chem. Phys. 95 (1991) 2965.
[3] M.B. Robin, I. Ishii, R. McLaren, A.P. Hitchcock, J. Electron Spectrosc. Relat. Phenom. 47 (1988) 53.
[4] S.G. Urquhart, H. Ade, J. Phys. Chem. B 106 (2002) 8531.
[5] C. Hannay, J. Heinesch, U. Kleyens, M.-J. Hubin-Franskin, Meas. Sci. Technol. 6 (1995) 1140.
[6] M.-J. Hubin-Franskin, H. Aouni, D. Duflot, F. Motte-Tollet, C. Hannay, L.F. Ferreira, G. Tourillon, J. Chem. Phys. 106 (1997) 35.
[7] M.-J. Hubin-Franskin, J. Heinesch, Nucl. Instrum. Methods A 477 (2002) 546.
[8] R.N.S. Sodhi, C.E. Brion, J. Electron Spectrosc. Relat. Phenom. 34 (1984) 363.
[9] D. Duflot, J.-P. Flament, I.C. Walker, J. Heinesch, M.-J. Hubin-Franskin, J. Chem. Phys. 118 (2003) 1137.
[10] G. Chaban, M.W. Schmidt, M.S. Gordon, Theor. Chem. Acc. 97 (1997) 88.
[11] M.W. Schmidt, K.K. Baldridge, J.A. Boatz, S.T. Elbert, M.S. Gordon, J.H. Jensen, S. Koseki, N. Matsunaga, K.A. Nguyen, S. Su, T.L. Windus, M. Dupuis, J.A. Montgomery Jr., J. Comp. Chem. 14 (1993) 1347.
[12] S. Bodeur, P. Millié, I. Nenner, Phys. Rev. A 41 (1990) 252.
[13] S. Carniato, Y. Luo, J. Electron Spectrosc. Relat. Phenom. 142 (2005) 163.
[14] B. Huron, J.P. Malrieu, P. Rancurel, J. Chem. Phys. 58 (1973) 5745.
[15] R. Cimiraglia, J. Chem. Phys. 83 (1985) 1746.
[16] S. Stranges, M. Alagia, G. Fronzoni, P. Decleva, J. Phys. Chem. A 105 (2001) 3400.
[17] C. Angeli, R. Cimiraglia, M. Persico, A. Toniolo, Theor. Chem. Acc. 98 (1997) 57.
[18] T.H. Dunning, J. Chem. Phys. 55 (1971) 716.
[19] T.H. Dunning Jr., J. Hay, in: H.F. Schaefer III (Ed.), Methods of Electronic Structure Theory, Plenum Press, New York, 1977, p. 1.
[20] J.P. Dognon, C. Pouchan, A. Dargelos, J.P. Flament, Chem. Phys. Lett. 109 (1984) 492.
[21] J.-P. Flament, Ph.D. Thesis, Université de Paris-Sud, 1981.
[22] L.S. Cederbaum, W. Domcke, J. Chem. Phys. 64 (1976) 603.
[23] H. Köppel, W. Domcke, L.S. Cederbaum, Adv. Chem. Phys. 57 (1984) 59.
[24] T.D. Thomas, L.J. Saethre, S.L. Sorensen, S. Svensson, J. Chem. Phys. 109 (1998) 1041.
[25] U. Hergenhahn, J. Phys. B 37 (2004) R89.
[26] D. Duflot, S. Zeggari, J.-P. Flament, Chem. Phys. 327 (2006) 518.
[27] A.B. Trofimov, E.V. Gromov, T.E. Moskovskaya, J. Schirmer, J. Chem. Phys. 113 (2000) 6716.
[28] R.B. Gerber, J.O. Jung, in: P.R. Bunker, P. Jensen (Eds.), Computational Molecular Spectroscopy, Wiley and Sons, Chichester, 2000, p. 365.
[29] J.L. Derissen, J. Mol. Struct. 7 (1971) 67.
[30] S. Shirai, S. Yamamoto, S.-A. Hyodo, J. Chem. Phys. 121 (2004) 7586.
[31] Y. Takahata, D.P. Chong, J. Electron Spectrosc. Relat. Phenom. 133 (2003) 69.
[32] W.L. Jolly, K.D. Bomben, C.J. Eyermann, At. Data Nucl. Data Tables 31 (1984) 433.
[33] T.D. Crawford, H.F. Schaefer III, T.J. Lee, J. Chem. Phys. 105 (1996) 1060.
[34] P.J. Knowles, J.S. Andrews, R.D. Amos, N.C. Handy, J.A. Pople, Chem. Phys. Lett. 186 (1991) 130.
[35] W.J. Lauderdale, J.F. Stanton, J. Gauss, J.D. Watts, R.J. Bartlett, Chem. Phys. Lett. 187 (1991) 21.
[36] T.J. Lee, D. Jayatilaka, Chem. Phys. Lett. 201 (1993) 1.
[37] T.J. Lee, A.P. Rendell, K.G. Dyall, D. Jayatilaka, J. Chem. Phys. 100 (1994) 7400.
[38] W.J. Hunt, I. Goddard, A. William, Chem. Phys. Lett. 3 (1969) 414.
[39] P.-O. Löwdin, Phys. Rev. 97 (1955) 1474.
[40] P. Norman, H. Agren, J. Mol Struct. (THEOCHEM) 401 (1997) 107.
[41] D. Duflot, J.-P. Flament, A. Giuliani, J. Heinesch, M. Grogna, M.-J. Hubin-Franskin, Phys. Rev. A 75 (2007) 052719.
[42] O. Takahashi, K. Tabayashi, S.-I. Wada, R. Sumii, K. Tanaka, M. Odelius, L.G.M. Pettersson, J. Chem. Phys. 124 (2006) 124901.
[43] K. Tanaka, H. Kizaki, R. Sumii, Y. Matsumoto, S. Wada, Radiation Physics and Chemistry, Proceedings of the 20th International Conference on X-ray and Inner-Shell Processes, vol. 75, Melbourne, Australia, July 4–8, 2006, p. 2076.
[44] H. Kizaki, Y. Matsumoto, H. Ban, K. Morishita, S.-i. Wada, K. Tanaka, Surf. Sci. 601 (2007) 3956.
[45] O. Takahashi, T. Matsui, A. Kawano, K. Tabayashi, K. Yamasaki, J. Mol. Struct. (THEOCHEM) 808 (2007) 35.
[46] S. Pilling, A.C.F. Santos, H.M. Boechat-Roberty, Astronom. Astrophys. 449 (2006) 1289.
[47] S. Pilling, H.M. Boechat-Roberty, A.C.F. Santos, G.G.B. de Souza, A. Naves de Brito, J. Electron Spectrosc. Relat. Phenom. 156–158 (2007) 139.